coatings

MDPI

Article

The Anti-Snow Behaviour of Icephobic Coatings: Laboratory and In-Field Testing

Marcella Balordi [1,*], Giorgio Santucci de Magistris [1], Alessandro Casali [1,2], Francesco Pini [1,3], Andrea Cammi [1], Matteo Lacavalla [4] and Vincenzo Rotella [4]

[1] RSE, Ricerca sul Sistema Energetico, Strada Torre della Razza, 29122 Piacenza, Italy
[2] Department of Chemical Science, Life Sciences and Environmental Sustainability, University of Parma, Parco Area Scienze 17/A, 43124 Parma, Italy
[3] Facoltà di Scienze Chimiche, Università Degli Studi di Pavia, viale Taramelli 12, 27100 Pavia, Italy
[4] RSE, Ricerca sul Sistema Energetico, via Rubattino 54, 20134 Milano, Italy
* Correspondence: marcella.balordi@rse-web.it

Abstract: Overhead power line conductors and ground wires are affected by ice and snow accretion which can easily adhere to their surface, causing the breakage of cables and the collapse of pylons due to excessive weight. In Italy, the main concern is about wet snow: this phenomenon occurs close to zero degrees Celsius with snow density reaching up to 350 Kg/m^3. Anti-icing and anti-snow coatings represent a possible strategy to mitigate ice accretion on overhead power line structures. Many works are oriented to achieve anti-icing properties, starting from superhydrophobic coatings or slippery coatings; however, there is a lack of knowledge about the anti-snow behaviour of these surfaces. In this work, aluminium alloy conductor and ground-wire samples were prepared with different coatings, which include hydrophobic, superhydrophobic and slippery surfaces prepared in the laboratory. Characterisations of sample wettability at room and low temperatures and ice adhesion strength were carried out in the laboratory. Anti-snow behaviour was studied in outdoor test facilities in the Italian Alps during several snowfall events. Furthermore, the environmental parameters were also recorded. Two figures of merit were developed to quantify anti-snow behaviour of the samples: one describing the fraction of surfaces covered by snow during the snowfall event and the other representing the maximum accretion load reached on the samples. Results of laboratory and field testing are compared and discussed. Field testing evidenced a promising snowphobic behaviour for all the samples, despite the different anti-icing and wettability properties measured in the laboratory. The mitigation of the phenomenon was found to occur mainly with two different mechanisms: the delay in snow accretion on the surface and/or the early shedding of the snow-sleeve.

Keywords: anti-snow coating; anti-icing coating; superhydrophobic; slippery; overhead power line conductors; ground wires; field testing

check for updates

Citation: Balordi, M.; Santucci de Magistris, G.; Casali, A.; Pini, F.; Cammi, A.; Lacavalla, M.; Rotella, V. The Anti-Snow Behaviour of Icephobic Coatings: Laboratory and In-Field Testing. *Coatings* **2023**, *13*, 616. https://doi.org/10.3390/coatings13030616

Academic Editors: Yizhou Shen and Emerson Coy

Received: 29 December 2022
Revised: 8 March 2023
Accepted: 10 March 2023
Published: 14 March 2023

Copyright: © 2023 by the authors. Licensee MDPI, Basel, Switzerland. This article is an open access article distributed under the terms and conditions of the Creative Commons Attribution (CC BY) license (https://creativecommons.org/licenses/by/4.0/).

1. Introduction

Overhead power lines are subjected to icing phenomena: ice and snow can gather on conductors and ground wires, hugely increasing the weight of the structures and causing the breakage of the conductors or, even worse, the collapse of the pylons [1].

Icing can happen in a wide range of climatic conditions: temperature, wind speed and air humidity are just some of the parameters that play a role in snow and ice accretion. Thus, ice accretions can widely differ from each other in weight, density and adhesion properties. For instance, in cold regions (e.g., Canada, China, Norway), the main problem concerns the formation of cylindrical ice masses accreted from in-cloud icing and rime [2] and is characterised by high density and hardness. On the contrary, in climatic zones with a more temperate climate, such as Japan, France, Spain, Italy and Slovenia, wet snow, in in the form of heavy coatings that wrap conductors and ground wires, is the most dangerous problem.

Wet snow is a peculiar kind of snowfall that happens in a range of temperatures from −1 °C to 2 °C, with a liquid water content (LWC) ranging from 15% to 35%. Due to the high LWC, this type of snow reaches an excessive weight and can easily adhere to the metallic surface of conductors or ground wires, creating a snow sleeve [3]. In the last few decades, wet snow accretions caused various blackouts and serious damage in northern Europe [4], and in 2015, this phenomenon hit several Italian regions, in particular the Emilia Romagna and Lombardy. At the end of that period, in February 2015, the Regulatory Authority for Energy Networks and the Environment (ARERA) conducted a fact-finding investigation (Deliberation 96/2015/E/eel) about the electricity supply interruptions caused by wet snowfalls in the most affected areas. The investigation highlighted a shortage in supplied energy to end-users for 990 MWh. This value, related only to the first 2 months of the year, represents approximately one-fifth of the average gross energy not being delivered due to outages in the 5-year period 2010–2014, which is just below 5600 MWh/year (Deliberation 644/2015/E/eel Annex A). It has been calculated that in a single day, 33 million euros were spent in compensations for the lack of energy supply for more than 8 h, the threshold set by ARERA, in addition to the costs of restoring structural damage and service charges [5].

In view of the significant damage caused by this phenomenon, it is urgent to study systems and technologies capable of mitigating the formation of ice sleeves as much as possible. The development of coatings with anti-icing and anti-snow properties is a promising strategy to address this problem [6]. Different coatings are studied to reach anti-icing performance and, among this wide range, superhydrophobic and slippery coatings receive the main attention [7].

The former are extensively studied thanks to the strong water repulsion and their ability of decreasing ice nucleation temperature or increasing ice nucleation time, leading to lower ice adhesion strength [8,9]. The latter, in particular SLIPS (Slippery Liquid Infused Porous Surfaces), show low contact angle hysteresis and low sliding angles and evidence impressive liquid repellency properties: these peculiarities are mainly due to the presence of a lubricant liquid infused in the substrate. They can act as icephobic surfaces and are considered promising materials for their remarkable stability in high humidity environments [10] and their capacity in lowering the ice adhesion strength.

Even if the literature is rich in studies on anti-icing surfaces [11–13], only a few works deal with the behaviour of anti-icing coatings in presence of snow [14]. In particular, the anti-snow coatings have not yet been thoroughly investigated and procedures to clearly assess snowphobicity are not established yet.

In this work, we present three different types of coatings: superhydrophobic, hydrophobic and slippery. The coatings were deeply characterised in the laboratory in terms of wettability both at room and low temperatures and with ice detachment tests. Coated samples of conductors and ground wires were exposed to real snowfall events in two testing sites in the Italian Alps: their behaviour under snowfall is presented here. This work shows that both indoor and outdoor characterizations are important to improve the understanding of snowphobicity of surfaces with different properties and structures. The mitigation of the phenomenon was found to happen mainly with two different mechanisms: the delay in snow accretion delay and/or snow-sleeve early shedding. The mechanisms arise from different coating structures and depend on meteorological conditions.

2. Materials and Methods

2.1. Materials

Flat plates (20 × 70 × 2 mm^3), bars (12 mm diameter × 100 mm length), conductor pieces (31.5 mm diameter × 0.75 m length) and ground wires (20 mm diameter × 80 m length) of aluminium alloy (6082) were used.

Dynasylan® SIVO CLEAR EC (FAS) coating was purchased from EVONIK (Essen, Germany); the composition is: fluoroalkylsilane (FAS) 2%, propan-2-ol 93% and dodecane 5%. Hexane (95%) and acetone (>99.5%) were purchased from Sigma Aldrich (St. Louis, MO, USA).

Dynasylan® 9896 was purchased from EVONIK and consists in an oligomeric short-chain alkylfunctional silane. Here, the coating was diluted in ethanol (1:1 in volume) before use.

Ethanol (99.5%), hexane (95%), acetone (>99.5%) and acetic acid (≥99.7%) Pluronic P-123, PDMS 750 cSt, PDMS 65 cSt, MTEOS (99%) were purchased from Sigma Aldrich (St. Louis, MO, USA).

Ultrapure water was used for synthesis and characterisations.

2.2. Samples Preparation

First, the aluminium alloy specimens were cleaned as follows: (1) bathing with basic soap; (2) rinsing in ultrasonic bath for 10 min with acetone; and (3) drying under nitrogen flux.

Starting from flat plates, several samples were prepared by applying different mechanical and chemical processes. The prepared samples were divided into three groups: superhydrophobic (SH), hydrophobic (HP) and slippery (SL) and named SH-1, HP, SL-1 and SL-2, respectively. The corresponding bars, conductor pieces and ground wires were also prepared, following the same steps.

2.2.1. Superhydrophobic Sample SH-1

In SH-1, a sandblasting process with micro glass beads in 40–70 μm diameter range, followed by a hydrothermal treatment in water at 100 °C for 30 min was performed to obtain a hierarchical micro-nano structure. Then, the surface was dip-coated with the FAS and cured at 70 °C for 1 h.

2.2.2. Hydrophobic Sample HP

The HP was easily prepared by dip-coating of the aluminium alloy samples in FAS and thermal treatment at 70 °C for 1 h.

2.2.3. Slippery Samples SL-1 and SL-2

For the preparation of SL-1, the aluminium alloy was immersed in boiling water for 30 min at 100 °C. Diluted Dynasilan® 9896 (1:1 in volume, solvent ethanol) was stirred for 1 h. The aluminium samples were dip-coated in the solution and cured at 120 °C for 1 h.

For the preparation of SL-2, a multistep process was completed. The different ratios among the reagents were tested with several reactions. Here, we report the best one in terms of wettability and icephobic behaviour. First, 0.15 g of Pluronic P-123 and 0.1 g of NaOH were added to 5 mL of water and stirred until the complete dissolution of Pluronic 123. The obtained solution (SOL_A) was aged for 1 h at 4 °C. PDMS 750 cSt, PDMS 65 cSt and MTEOS (0.9 g; 2.5 g and 8.4 g, respectively) were mixed (MIX_A). The SOL_A was then added to MIX_A and the resulting mixture was magnetically stirred for 30 min. Further, the aluminium alloy sample was dip-coated into the mixture and cured at 120 °C for 2 h.

2.3. Indoor Characterisation

Surface morphologies of all the samples and the thickness of the oxide layers were examined using a field emission scanning electron microscope (FE-SEM; Mira III, Tescan, Brno, Czech Republic).

A Taylor Hobson mechanical profilometer was used to measure surface roughness, data are averaged over at least 5 runs for each sample.

The analysis of the nanostructure was carried out with the atomic force microscope (AFM, DriveAFM, Nanosurf, Liestal, Switzerland) with clean-drive tapping mode analysis.

The FT-IR characterizations were conducted with the FT-IR Alpha 1 (Bruker, Billerica, MA, USA country) spectrometer with ATR apparatus (diamond crystal was used as the internal reflection element).

The static water contact angles (WCA) were measured with the DSA 30 Drop Shape Analyzer (Kruss, Hamburg, Germany) with the method of the sessile drop using 4 μL of water at 23 °C ± 2 °C on at least 5 spots for each sample. The measurements of dynamic

contact angles (advancing and receding contact angles), roll-off angles (RA) and sliding angles (SA) were performed with the tilting table method [15] using 20 µL of water at 23 °C ± 2 °C.

WCA, dynamic contact angles and RA/SA measurements at low temperatures were conducted with two different instrumental settings. In setting 1 the sample was placed on a Peltier plate in a climatic chamber (Kruss, Hamburg, Germany), cooled at −4 °C and then the drop was deposited on the cooled sample. In setting 2, suggested by [16,17], the sample was inserted into the climatic chamber together with a beaker filled with water. The sample was placed on a sample holder above the Peltier cell. The drop was deposited on the sample at room temperature and after 15 min the temperature was decreased at a rate of 0.3 °C/min until −4 °C. For WCA measurement 4 µL and 10 µL water drops were used with setting 1 and 2, respectively, on at least 5 spots for each sample. The measurements dynamic contact angles at −4 °C were performed increasing and decreasing the volume of a sessile drop and to measure RA and SA at −4 °C, the Peltier chamber was attached to a homemade tilting table, and 20 µL water drops were used on at least 3 spots for each sample.

Ice adhesion strength was evaluated using the shear force needed to extract a sample bar from an ice block. We adopted a homemade apparatus equipped with an electromechanical testing system (INSTRON 4507) and aluminium alloy bars were used as test samples. The measures were carried out at −19 °C. The testing process and the apparatus are described in the Supplementary Materials section. The shear stresses were calculated as an average of 5 tests carried out on 5 different specimens for each treatment. For comparison purpose, the shear stress of bare aluminium alloy bars was measured too.

2.4. Snowphobic Evaluation

The coated conductor specimens were installed on the RSE automated monitoring station named WILD (Wet Snow Ice Laboratory Detection) [18] and monitored during the winter season. Qualitative tests were carried out by verifying the ability of conductors treated with icephobic coatings to delay the formation or to quicken the detachment of snow sleeves, with respect to the uncoated specimen, in the same snow conditions.

2.4.1. Description of the Outdoor Test Facility

The WILD station, located in the Western Alps, has been operating since 2013. The main objective is to monitor the effect of wet snow over conductors, ground wires and insulator specimens. The WILD facility consists of a meteorological station able to record several parameters like the minimum and maximum temperature, wind speed, cumulated precipitation and the maximum precipitation rate. A top view picture of the station and the specific instrumentation for monitoring the meteorological variables are detailed in the Supplementary Materials.

WILD mainly consists of two stations, dedicated to the installation and the monitoring of specimens of conductors and ground wires, ranging in a length from 0.75 to 15 mt Figure 1. Both the stations are equipped with mechanical rotation supports to transmit a slow rotation, as suggested by the ISO 12494:2017 standard. The slow rotation (1 rotation every 30 min) simulates the natural rotation of real conductors or ground wires, which is essential to the formation of the snow-sleeve, as explained by several snow-sleeve accretion models [19–22].

Each testing station is equipped with a dedicated webcam for monitoring the snow sleeve formation and detachment, through the acquisition of images every 15′. As reported in Figure 1, in WILD, it is possible to host and monitor up to 6 long conductors of approximate length of 15 m and up to 10 ACSR (Aluminium Conductor Steel Reinforced) 75 cm conductor specimens. One of the reference conductor samples is also equipped with a load cell measuring the weight of the accreted snow sleeve. It is also possible to host and monitor up to 4 insulator chains.

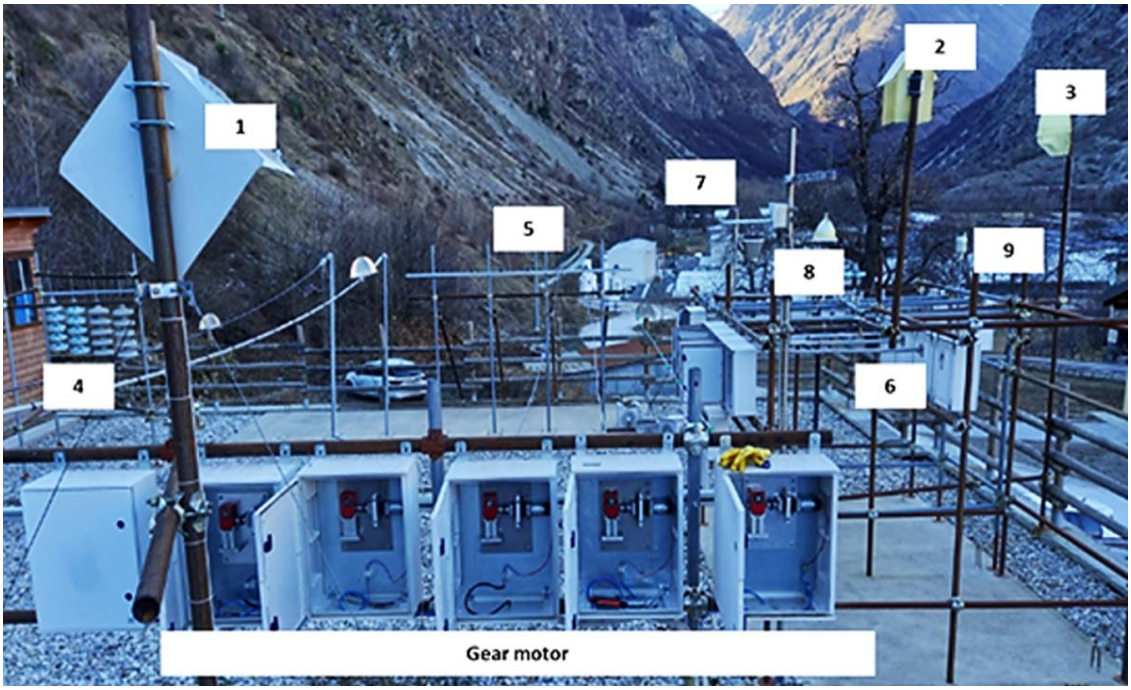


Figure 1. WILD station and the equipment. 1,2,3: webcam motobix; 4: insulator testing station; 5: 15 mt span conductor testing station; 6: 1.5 mt pieces conductor testing station; 7: anemometer; 8: rain gauge; 9: Vaisala multisensor.

2.4.2. Evaluation Method of Field Performances

The coated samples were mounted on the housing system described above, along with an uncoated sample, used as a reference, and the images acquired at each time stamp were analysed to estimate their snow coverage index (cov). Cov is a number between 0 and 1 which accounts if the wire is totally free of snow (0 value), or completely covered (1) or any intermediate value.

To give a representation of the behaviour of each sample during the snow event, two figures of merit were defined [23]: the Relative Coverage index (RCov) and the Mitigation Load Index (MLI). RCov can be calculated from the coverage data, as the sum of the cov values in each time stamp and normalizing the total with respect to the reference sample, as follow:

$$\mathrm{Rcov} = \sum_n \mathrm{cov}_n \Big/ \sum_n \mathrm{covRef}_n \quad (1)$$

RCov compares the coated samples and the reference. Values lower than 1 are therefore attributed to samples that perform better with less snow coverage and values greater than 1 to samples with worse behaviour than the reference.

The MLI indicates the maximum weight reached by a coated conductor during the snow event, in respect to the reference. This can be estimated as a function of the precipitation rate and depending on the coverage index. First, we estimated the relative load (ERL) for each conductor, adding the load already present on the sample at time n-1 or subtracting the amount that sheds as follows:

$$\mathrm{ERL}_n = \mathrm{cov}_n \times \mathrm{PR}_n + \mathrm{ERL}_{n-1} \ (\text{if } \mathrm{cov}_n \geq \mathrm{cov}_{n-1}) \quad (2)$$

$$\mathrm{ERL}_n = \mathrm{cov}_n \times \mathrm{PR}_n + \mathrm{ERL}_{n-1}/\mathrm{cov}_{n-1} \times \mathrm{cov}_n \ (\text{if } \mathrm{cov}_n < \mathrm{cov}_{n-1}) \quad (3)$$

where:

cov_n is the coverage index at the moment n

PR_n is the precipitation rate at the moment n

MLI can be obtained from the ERL values, considering the maximum value reached by each sample with respect to the reference.

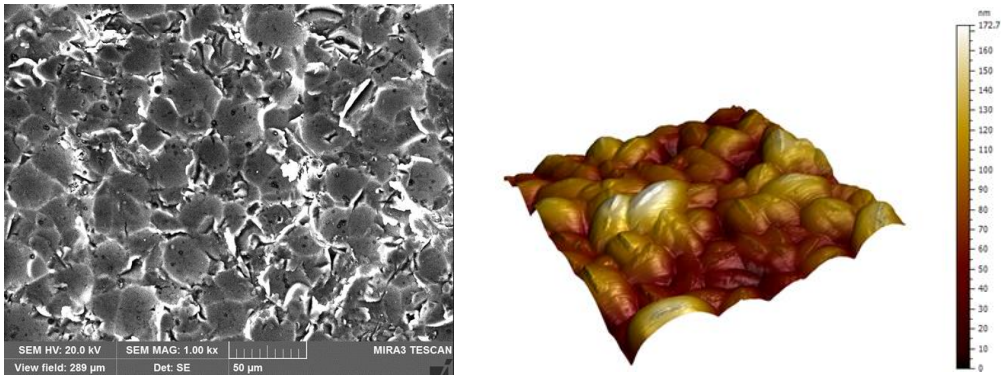
$$\text{MLI} = \max \text{ERL}_{\text{sample}} / \max \text{ERL}_{\text{reference}} \quad (4)$$

The smaller the MLI the better the snowphobic behaviour of the coating. Simplifying, RCov and MLI aim to evaluate and quantify the ability of a coating to delay the formation of the snow-sleeve and to facilitate the shedding of the snow.

3. Results and Discussion

3.1. Morphological and Chemical Evaluation

The SH-1 morphology is reported in Figure 2. The surface evidences a micro-roughness due to the sandblasting treatment (Figure 2a). The calculated Ra is 0.94 µm. After the hydrothermal treatment, a pseudo-boehmite layer grew on the surface, leading to the typical grass-like nanostructure [24], the SEM image is reported in the Supplementary Materials. According to the equation presented in [25] and reported in the Supplementary Materials, a thickness of about 500 nm was estimated for the oxide layer. The nano-roughness of the pseudo-boehmite was about 28.6 nm (S_a) and the AFM image of the nanostructures is reported in Figure 2b.



(a) **(b)**

Figure 2. (**a**) SEM image of the micro-roughed surface (SE, 1 kx), (**b**) AFM image of the nanostructure (1 µm × 1 µm) tapping mode, 3D rendering.

The FAS coating is deposited on the surface of the specimen in a very thin layer of about 1.5 nm [26], and its presence on the surface is confirmed by FTIR spectra (Supplementary Materials).

The HP sample evidences a native roughness of 0.3 µm (Ra) due to the pristine substrate (Figure 3).

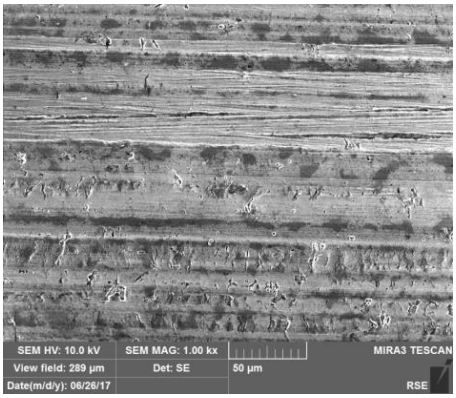


Figure 3. SEM image of the HP surface (SE, 1 kx). The native roughness is well visible.

Two different slippery surfaces were prepared: SL-1 and SL-2. In SL-1, the aluminium surface is functionalised with a 1 µm thick layer of oligomeric short alkyl chains whereas SL-2 is a polymeric material formed by interaction among siloxane precursor and PDMS chains and intercalated with the Pluronic.

As described in our previous work [27], in SL-1, the coating fills up the voids in the nanostructured layer and the surface is almost totally covered by the coating. On this surface, the pseudo-boehmite has a double function: (i) enhancing the adhesion between the substrate and the coating, thanks to the formation of Al–O–Si bonds; and (ii) increasing the porosity of the surface allowing to host a bigger amount of coating respect to an untreated surface.

The SL-2 sample was synthetised by a sol-gel reaction between MTEOS and hydroxy-terminated PDMS in a basic catalyst, followed by the addition of Pluronic. As reported in the literature [28], the basic catalyst leads to the hydrolysis of the Et–O–Si bonds of MTEOS and further, the polycondensation of the hydrolysed silane happens. The polycondensed silane reacts with the terminated HO–Si group of the PDMS, giving rise to a complex multibranched polymeric structure, where silica nanoparticles are branched with PDMS chains, as represented in Figure 4.

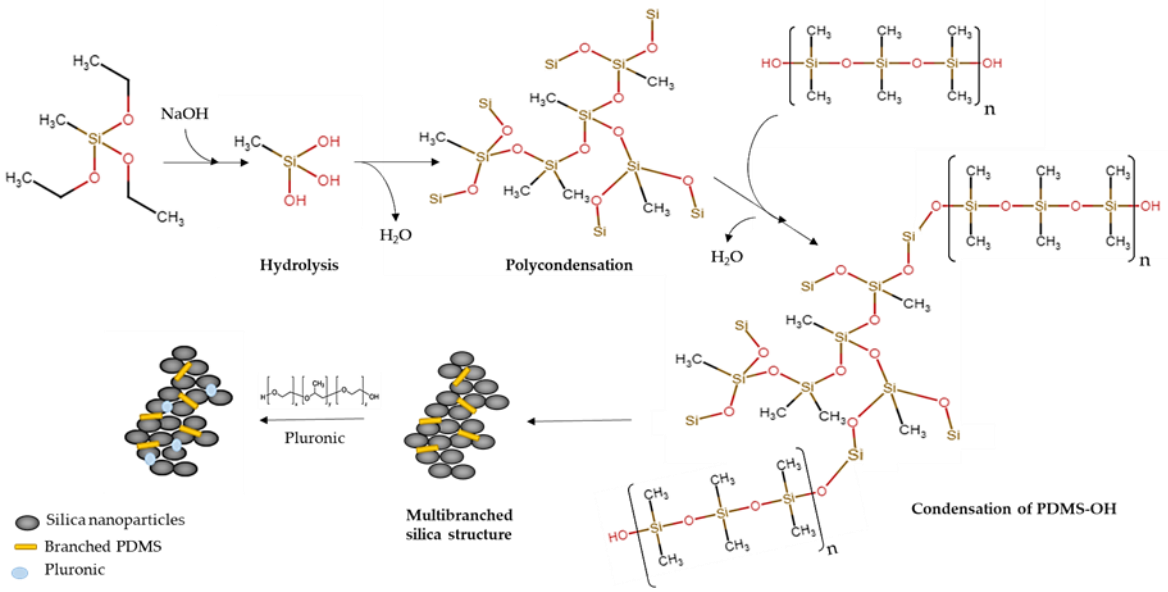


Figure 4. Reaction between MTEOS, PDMS-OH and Pluronic.

Pluronic polyols represent a class of block copolymers, consisting of poly(oxyethylene) and poly(oxypropylene) units, with the general formula poly(oxyethylene)$_x$-poly(oxypropylene)$_y$-poly(oxyethylene)$_z$. Pluronic sits among the PDMS chain. Pluronic has a peculiar gel–sol phase transition due to presence of more hydrophobic moieties in its structure that interact with water molecules creating a solution only at low temperatures, when kinetic energy of water molecules is low [29]. Under a certain temperature, Pluronic becomes a solution, unlike most materials which behave reversely. This effect has been exploited to obtain a material which forms a water quasi liquid layer at low temperature only [30].

The FTIR of the polymer is reported in Figure 5. The signals at 781, 1007 and 1082 cm^{-1} are attributed to Si–O–Si and Si–O–C. The signals at 1258 cm^{-1} and 864 cm^{-1} are typical for Si–C stretching, at 2963 cm^{-1} are the signals of C–H stretching of methyl groups. From 2904 to 2871 cm^{-1} the signals can be attributed to the unreacted O–CH_2–CH_2 groups and stretching vibration of C–H methylene group. The broad peak at about 3400 cm^{-1} is related to the to the O–H stretching vibration in water molecules interacting via hydrogen bonds [31,32].

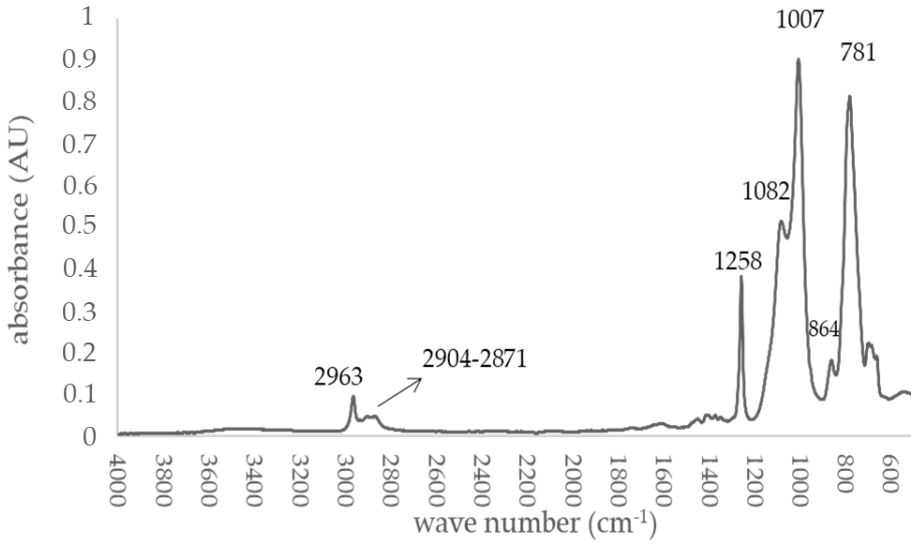


Figure 5. FTIR spectra of SL-2.

3.2. Wettability at Room Temperature

In order to study the wettability of the samples, we measured the WCAs, the hysteresis values (H), calculated as the difference between advanced and receding angles, and the RAs and SAs of the surfaces. From the WCA values, it is possible to define if a surface is hydrophobic or hydrophilic (>90° and <90°, respectively). H and RA/SA angles represent two crucial parameters to understand how easy a water droplet deposed on the surface can be removed. The WCA, the H and the RA/SA results are collected in Table 1.

Table 1. Wettability at 23 °C ± 2 °C and standard deviation.

Sample	WCA (°)	H (°)	RA/SA (°)
SH-1	171.4 ± 1.0	2.6 ± 0.8	1.7 ± 1.2
HP	111.2 ± 1.5	68.2 ± 2.8	>90
SL-1	86.7 ± 1.5	2.0 ± 0.1	2.0 ± 0.2
SL-2	89.8 ± 5.3	18.7 ± 1.4	6.7 ± 0.5

SH-1 evidences a high WCA (>150°) and very low water adhesion (H and RA/SA < 10°). These results are typical of superhydrophobic materials where a micro-nano hierarchical surface is coated with a hydrophobic coating, as explained by the Cassie–Baxter model [33].

The role of the hierarchical structure is crucial to achieve superhydrophobicity and the corresponding sample without this underlying structure (HP) shows lower WCA. Indeed, the wettability of the sample can be described by Wenzel model [34], as the hydrophobicity of this sample is only due to the low surface energy of FAS coating. While the surface exhibits hydrophobic behaviour (WCA > 90°), it also demonstrates high water adhesion.

The behaviour of SL-1 and SL-2 is very similar: at room temperature, the WCAs of both materials indicate a state between hydrophilic and hydrophobic conditions. Despite this, they show low water adhesion with low H and SA values. Although the SL-1 is not definable SLIPS [27], the H and SA are very low and completely comparable with SLIPS surfaces [35]. The behaviour of SL-2 can be mainly attributed to the presence of Pluronic which is a liquid part that sits among the silicon polymeric chain.

3.3. Wettability at Low Temperature

The behaviour of coatings at low temperature may vary from room temperature and can be more significant when seeking icephobicity [36,37]. As wettability is sensitive to the set-up used for measurement, both settings described in chapter 2.3 were used. In Table 2, the WCA, H and RA/SA at −4 °C are reported.

Table 2. Wettability at low temperature (−4 °C) and standard deviation.

Sample	Setting 1			Setting 2		
	WCA (°)	H (°)	RA/SA (°)	WCA (°)	H (°)	RA/SA (°)
SH-1	146.8 ± 1.7	13.9 ± 2.7	>90	159.2 ± 2.1	22.6 ± 6.1	15.6 ± 5.9
HP	106.7 ± 1.5	66.4 ± 11.4	>90	110.4 ± 1.2	60.4 ± 7.2	>90
SL-1	81.5 ± 0.9	8.6 ± 0.8	16.0 ± 2.0	90.8 ± 0.5	8.5 ± 1.2	16.2 ± 2.6
SL-2	82.0 ± 1.6	30.9 ± 1.4	14.3 ± 0.5	87.3 ± 2.1	28.6 ± 2.3	12.5 ± 1.1

In setting 1, water was deposited on the cooled sample directly laid on the Peltier plate. By placing the sample in thermal contact with the cooling plate, the surface of the sample is prone to air humidity condensation. This causes a strong degradation of hydrophobic properties for HP and SH-1. In particular for SH-1, the condensation layer reduces the volume of the air pockets incorporated in the hierarchical surface, which are linked to the rise of superhydrophobic properties, as discussed in several works [16,36,38].

In setting 2, both the sample and the water drop were thermally insulated from the cooling plate, reaching the final temperature only by exchanging heat with the surrounding air. The system was also cooled at a slow rate (0.3 °C/min) which allowed the water in the beaker to stabilise humidity in the chamber. Due to this, condensation on the sample is avoided. The wettability of the samples, measured with setting 2, evidenced values very close to those collected at room temperature. In particular, the hydrophobic behaviour of SH-1 is preserved and resulting in WCA of about 160° and good dynamic properties. This experiment proved that the worse wettability behaviour of SH-1 and HP measured with setting 1 is mainly due to the formation of humidity condensation.

Noteworthily, SLs keep a low sliding angle at low temperatures regardless of the measurement setting. This behaviour indicates that the SLs coatings better tolerate the different cold conditions and humidity condensation phenomena, similarly to SLIPS coatings [35], demonstrating robustness towards both applied conditions. Probably, this is due to the absence of impurities and surface defects which are very likely to be present on smaller surface area in respect to the rough superhydrophobic surface when exposed to condensed humidity. Moreover, in SL-2 the presence of the Pluronic lead to the formation of a quasi-liquid layer which helps to maintain a low sliding angle [30,39].

3.4. Ice Adhesion Tests

The icephobic properties of the samples were tested by measuring ice adhesion. Adhesion reduction factor (ARF), the ratio between average shear stress ($\overline{\tau}$) of bare aluminum alloy and average shear stress of coated sample, was also calculated.

$$\mathrm{ARF} = \overline{\tau}_{bare} / \overline{\tau}_{sample} \quad (5)$$

The higher the ARF values, the higher the icephobic properties of the tested samples. Results are reported in Table 3.

Table 3. Shear stress values and ARF of the tested samples. The shear stress of bare aluminium alloy is 1009 ± 230 kPa.

Sample	Shear Stress (kPa)	ARF
SH-1	92 ± 18	11.0
HP	804 ± 76	1.3
SL-1	43 ± 14	23.5
SL-2	71 ± 36	14.2

The superhydrophobic sample reduces ice adhesion by 11 times compared to the bare sample. This result highlights a great icephobic behaviour to several superhydrophobic and hydrophobic examples in literature measured with similar techniques [40–43]. The

hierarchical micro-nano structure is crucial to achieve icephobicity. Indeed, the HP shows only a small reduction in the ice adhesion with an ARF of 1.3 and the slight reduction in ice adhesion is due to the FAS coating. Ice adhesion data of SH-1 and HP confirm the relationship between wettability and icephobicity reported in several studies [41,44,45].

The slippery materials evidence the best icephobic behaviour, even better than the SH-1. The properties of SL-1 and SL-2 may be mainly due to the low H and SA even at low temperature [45,46].

3.5. Snowphobic Evaluation

ACSR conductor pieces 0.75 m long were prepared as described in 2.2 and exposed at the WILD station during the winter 2020–2021. An untreated conductor was also exposed and used as reference material for comparison purpose. The Figure 6 shows the conductor specimens and a typical experimental setup.



(a) **(b)**

Figure 6. (**a**) Pieces of conductor 0.75 m long; (**b**) typical experimental set-up in WILD station.

During the testing period, nine snowfall events were recorded at the WILD station from December to April. The main meteorological and physical variables of snowfall events are reported in Table 4 (see Supplementary Material for further data).

It is possible to classify the snowfall events as dry snow (d), wet snow (w) and dry–wet snow (dw). In dry snow, the snowflake has a low liquid content and a high volume of air. This typically happens at temperatures below −1 °C. Wet snow typically occurred at temperatures around 0 °C and snowflakes have a high content of water inside. Dry–wet snow is a mixing phenomenon and a transition from dry to wet snow or vice versa may happen due to changes in the meteorological conditions.

Even if temperature is an important parameter, very often is not enough to correctly classify the type of snowfall. Other important parameters to take in account are the H_{snow} and WE. The H_{snow} is the height of the snow fallen on the ground and the WE represents the water equivalent of the snowfall. A low H_{snow}/WE ratio corresponds to wet snow, whereas a high ratio is very often related to dry snow. It is important to note that the WE parameter also gives information about the intensity of the snowfall.

Table 4. Main meteorological parameters of the snowfall events (T_{ave}: average temperature; WE: water equivalent; H_{snow}: height of snow deposition on the ground).

Number of Event	1	2	3	4	5	6	7	8	9
T_{ave} [°C]	−1.3	−0.3	−3.7	−0.6	−0.5	0.1	0.8	0.8	−0.4
WE [mm]	45.8	12.2	12	26.8	22.8	20	17.4	9.8	8
H_{snow} [mm]	420	190	170	270	240	165	41	25	110
Dry/wet	d	dw	d	dw	dw	dw	w	w	d

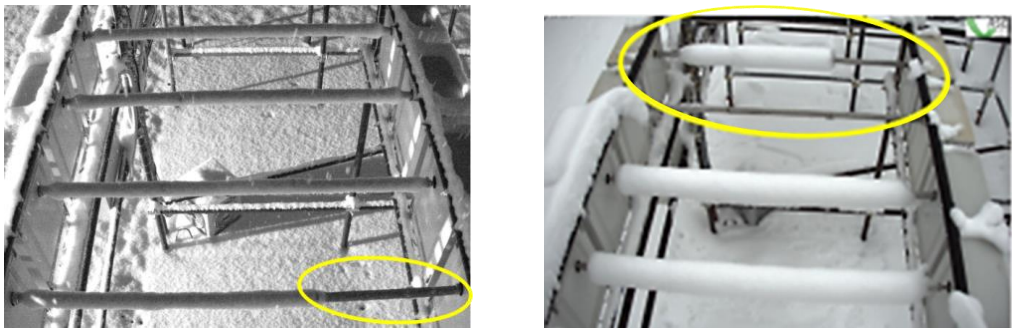
All the snowfall events led to the formation of the snow-sleeves on the rotating conductors. A lack of snow sleeve formation is likely due to a rotary engine failure which does not provide the proper rotation movement necessary for the growth.

In Figure 7, a typical snow sleeve on the reference conductor is reported.



Figure 7. Snow-sleeve on the reference conductor after a snow-fall event.

The anti-snow behaviour of the coated samples was always appreciable, and it manifested with two mechanisms: the delay in the formation of the snow-sleeve and the early detachment with respect to the reference. Example of these behaviours is reported in the Figure 8a,b, respectively.



(a) **(b)**

Figure 8. (**a**) Snow-sleeve in formation on the testing samples. A piece of conductor that delay the snow accretion is highlighted in yellow during a snowfall; (**b**) snow-sleeve after a snowfall event. The early shedding of the snow from the conductors is highlighted in a yellow circle.

The estimation method for MLI was assessed by comparing the calculated load profile ERL to the data from the load cell for the reference sample during a snow event (Figure 9). The ERL well represents the trend for both the loading and the detachment of the snow sleeve. In the second part of the event (from 1000 min until the end), the density of the snow increased, causing the difference between the real and the calculated snow-weight.

As the snow density is the same for all the exposed samples, the calculated ERL is considered to give a reasonable qualitative figure of the accreted sleeves on the samples.

In Tables 5 and 6, we collect the RCov and the MLI of the tested samples, compared to the reference (Ref).

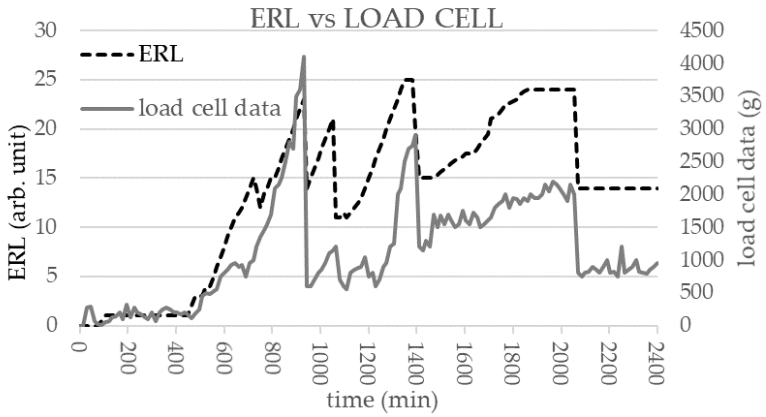


Figure 9. ERL and load cell data of the reference sample versus time during a snow event.

Table 5. Rcov index for the tested samples during the snowfall events. n.a data are not available.

Event	1	2	3	4	5	6	7	8	9	RCov Average
Type	d	dw	d	dw	dw	dw	w	w	d	
Ref	1.00	1.00	1.00	1.00	1.00	1.00	1.00	1.00	1.00	1.00
SH-1	0.52	0.85	0.18	0.62	0.28	0.90	0.75	0.90	0.99	0.67
HP	0.55	0.85	0.46	1.01	0.28	1.08	0.34	0.53	0.71	0.65
SL-1	0.38	0.99	0.59	0.98	0.61	1.12	0.34	0.38	0.81	0.69
SL-2	0.47	0.69	0.53	0.85	0.44	1.02	n.a.	n.a.	0.73	0.68

Table 6. MLI index for the tested samples during the snowfall events. n.a data are not available.

Event	1	2	3	4	5	6	7	8	9	MLI Average
Type	d	dw	d	dw	dw	dw	w	w	d	
Ref	1.00	1.00	1.00	1.00	1.00	1.00	1.00	1.00	1.00	1.00
SH-1	0.48	0.84	0.25	0.63	0.68	1.01	0.53	0.93	0.48	0.65
HP	0.38	0.51	0.90	0.45	0.64	1.01	0.70	0.85	0.49	0.66
SL-1	0.31	0.51	0.90	0.45	0.61	1.01	0.70	0.62	0.58	0.63
SL-2	0.54	0.56	0.83	0.44	0.64	1.01	n.a.	n.a.	0.47	0.64

Overall, the coated samples showed a reduction in snow accretion compared to the uncoated reference, as indicated by both the RCov and MLI indexes. Interestingly, the samples exhibited snowphobic properties even during heavy snowfalls (events 1, 4, and 5), regardless of snow intensity. However, the samples did demonstrate some variations in performance depending on the type of snowfall (dry, wet, or dry–wet).

In dry conditions, SH-1 demonstrated excellent performance, with a minimum RCov of 0.18 and a corresponding MLI of 0.25. This suggests that the coating was able to maintain a snow-free surface for a longer duration compared to the uncoated reference. Notably, even in event 9 where the RCov was high (close to 1), the MLI was 0.48, indicating that the coating facilitated snow detachment. Although SH-1 shows excellent performance in dry conditions, its snowphobic properties diminish in wet conditions (events 7 and 8) and in some dry–wet events where the temperature was just below zero (event 2 and 6). Despite this, it still mitigates the formation of the snow sleeve compared to the reference, except for event 6.

Both the slippery samples show good anti-snow properties under dry snow: both the RCov and MLI indexes are below the reference by at least 10%. SL-1 assessed its anti-snow behaviour also under wet-snow events with a very low RCov and MLI (events 7 and 8). Unfortunately, the data during the wet-snow events are not available for SL-2 due to the failure of the rotation motor. However, the performances recorded during the dry–wet

snowfall events were good and the results obtained with the coating with similar wettability properties (SL-1) are suggest that the proposed treatment is a promising one even in wet-snow conditions, although further tests will need to be conducted. The HP sample evidences no clear similarity in its snowphobic behaviour with SH-1 or with the slippery coating, performing in a fluctuating way under dry, wet and dry–wet events.

3.6. Relationship among Wettability, Icephobicity and Snowphobicity

A comparison among the wettability, the icephobicity and the snowphobicity of the tested sample was performed. A clear correlation among these properties is not possible; however, some considerations can be drawn.

First, icephobicity is not a necessary condition to achieve the snowphobicity; indeed, the sample HP evidenced poor anti-ice properties but good anti-snow behaviour.

Moreover, the study suggests that the static contact angle is not a reliable predictor of the anti-snow behaviour. Despite the tested samples exhibiting a range of WCAs from 86.7° (for SL-1) to 171.4° (for SH), covering the entire hydrophobicity spectrum, there was no observed correlation between WCA and MLI/RCov. This indicates that all samples showed a similar average snowphobicity, regardless of their WCA. However, it is important to note that under wet-snow conditions, SL-1 and HP performed better than SH-1 in terms of RCov. This behaviour may be attributed to the varying mobility of water observed at low temperatures. As explained in Section 3.3, SL-1 displayed favourable behaviour at low temperatures regardless of humidity, whereas condensation phenomena on the surface of SH-1 greatly impacted the mobility of water droplets, resulting in the loss of their dynamic properties as demonstrated by the wettability measurements conducted using setting 1. During a snowfall event, the thermal relationships between air/conductor/snow are complex and far from equilibrium; thus, condensation traces are likely to be found on the conductors' surface. Given that the snowflake has a high liquid water content (typically around 15%–35%) during a wet-snow event, the snow slides on the conductor and easily detaches from the surface for SL-1; conversely, the liquid water in the snowflake sticks to SH-1. With respect to HP, this effect is also magnified by the high surface area of SH-1 due to the micro-nano roughness.

Under dry conditions, the calculated RCovs are completely comparable among SH-1, HP, SL-1 and SL-2, and the best MLI is obtained for SH-1. This indicates that the different coatings have the same average snow coverage but that the shedding of the snow is facilitated on the SH-1 with respect to the other. RCov and MLI data, grouped by type of snow event, are presented in Figure 10.



Figure 10. RCov and MLI for the samples under wet-snow and dry-snow conditions (average data).

3.7. Snowphobic Test on Real Size Samples

Due to their good anti-snow behaviour observed in the WILD station, SH-1 and SL-1 were chosen for scaling up and testing in a section of a real overhead powerline (OHL) located in the Italian Alps at 1500 m above sea level. Ground wires that were 80 m long were prepared with SH-1 and SL-1 and installed on pylons 60 m high. The monitoring facilities and instruments mounted on the site are thoroughly described in [47]. In Table 7, the meteorological conditions of the snowfall events are reported.

Table 7. Meteorological conditions of the snowfall events.

SNOW EVENTS	A	B	C	D
TEMP MIN (°C)	−1.5	−1.8	0.0	0.0
TEMP MAX (°C)	1.3	1.1	1.5	0.1
TEMP AVE (°C)	0.1	−0.1	0.2	0.1
WE (mm)	40	15	20	70
PREC RATE MAX (mm/h)	3.4	2.4	7.4	7.8

Both events A and B, as well as C and D, occurred on 2 consecutive days. Event A started at −6 °C and then the temperature increased, settling at about 0 °C. Then, the precipitation stopped and the temperature increased. In event B, the precipitation started at about 0 °C and finished at −1.8 °C. At the beginning of event C, the recorded temperature was 1.5 °C and the conditions were rainy. Then, the temperature decreased, and settled at 0 °C throughout the event D.

In Table 8, we report the RCov and MLI indexes and in Figures 11 and 12 the estimated load calculated during the events is shown.

Table 8. RCov and MLI for SH-1 and SL-1.

SAMPLE	EVENT A		EVENT B		EVENT C		EVENT D	
	RCov	MLI	RCov	MLI	RCov	MLI	RCov	MLI
Ref	1	1	1	1	1	1	1	1
SH-1	0.44	0.23	0.65	0.49	0.54	0.59	0.08	0.09
SL-1	0.85	0.72	0.82	0.62	0.88	0.95	0.34	0.32

All the tested samples performed better than the reference and SH-1 is better than SL-1. In these experiments, SH-1 demonstrated promising anti-snow behaviour even with a temperature slightly above zero and under abundant snow fluxes.

ERL data suggest that the coating prevents the deposition of snow on the surface. Therefore, compared to the reference, the sample remained free from snow for a long time, and consequently, the snow-sleeve formed was thinner. During events C and D, reported in Figure 12, remarkable anti-snow behaviour was demonstrated for sample SH-1. Snow accretion was delayed for long time with respect to the reference; for event C, the delay was estimated being more than 1 h, for event D, it was about 2.5 h.

Figure 11 depicts that SH-1 experienced recurring shedding phases, characterised by frequent detachment of sleeve fragments from the wire, followed by loading phases. In contrast, SL-1 allowed for the detachment of snow at a "critical" weight, rather than having frequent shedding phases like SH-1. The observation from 1700 to 2050 seem to demonstrate a slightly better performance for the reference sample; however, this behaviour can be attributed to a casual event as, for instance, a gust of wind or a vibration due to random factors, are more likely to occur in natural environment.

The performance of both coatings is better in a real-scale overhead line (OHL) with an 80 m long guard wire compared to the WILD station with samples only 0.75 m long. This could be due to the higher mobility of the 80 m long sample, as well as the wind and vibrations from the surrounding environment, which are more effective in causing

shedding. Therefore, the efficacy of the coatings is more clearly visible in real-scale spans for all samples.

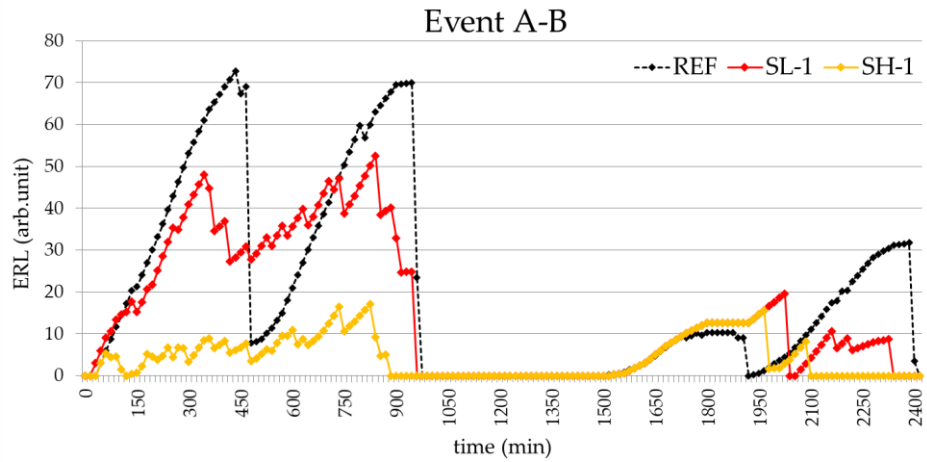


Figure 11. Calculated ERL during event A and event B.

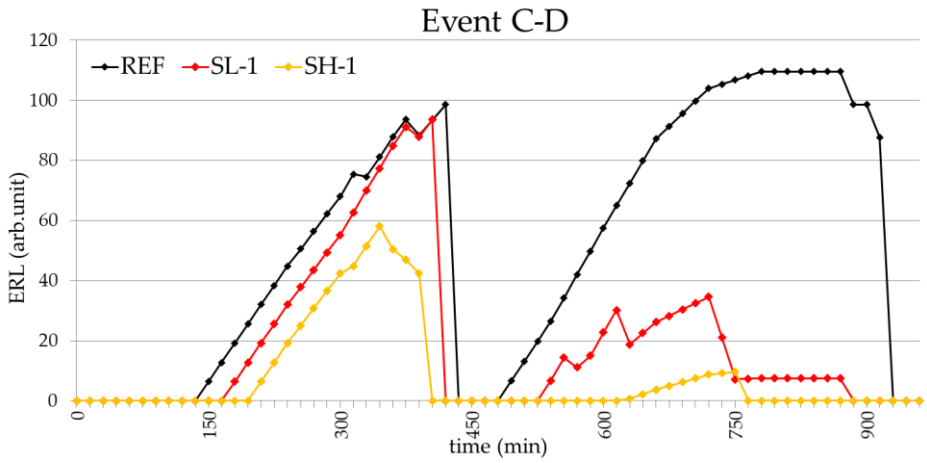


Figure 12. Calculated ERL during the events C and D.

4. Conclusions

Several samples with different coatings for anti-snow protection were prepared and tested in laboratory and exposed to real snow events in two sites in the Italian Alps. The coatings were characterised by different wettability and icephobicity: superhydrophobic, hydrophobic and slight hydrophilic with very good and low anti-icing behaviour were studied.

In order to obtain a quantitative dimension of sample performance during precipitations, two figures of merit were developed: one was related to the snow coverage of the sample surface and the second was related to the maximum load of the accreted sleeve with respect to the reference samples. The method of calculation of the accreted load was based on the coverage and the precipitation rate and the calculated load was compared with data obtained from a load cell mounted on a reference sample. A good agreement was found.

Comparison of indoor characterisation and field data demonstrates that the behaviour of the surfaces in real conditions is not clearly predictable from laboratory characterisation results. Even if a clear correlation has yet to be found, some interesting results were achieved. First, all the samples showed an anti-snow effect, even if not all of them have anti-ice properties. Thus, icephobicity is a sufficient but not necessary property to obtain anti-snow materials. Second, wettability at room temperature seems to be not very incisive for anti-snow properties; indeed, all the tested samples from superhydrophobic to hydrophilic ones are snowphobic.

However, samples with different SA/RA ratios at low temperatures exhibit different behaviour under wet snow. Specifically, SL-1 shows better performance under wet snow compared to SH-1, which performs better under dry snow. The superior behaviour of SL-1 is demonstrated by the RCov measurement: at the beginning of the wet-snow event on the SL-1 sample, the snow coverage was delayed. This could be attributed to the low SA angle, which is maintained even at temperatures as low as 0 °C, thereby facilitating the sliding of wet snow. In contrast, SH-1 exhibits poor dynamic properties below 0 °C, as the wet snow is likely to become trapped on its micro-nano rough surface. Further analysis of laboratory and field-testing data can be performed searching for correlation with meteorological conditions as, for instance, temperatures, wind and snow density.

Although a complete understanding of snow adhesion phenomena has not yet been achieved, the studied samples demonstrated good anti-snow properties even in real-scale spans, indicating that they hold promise for addressing the problem of snow accretion.

Supplementary Materials: The following supporting information can be downloaded at: https://www.mdpi.com/article/10.3390/coatings13030616/s1, Figure S1: Schematic representation of the shear stress home-made apparatus and a picture of the tensile machine used, Figure S2: WILD outdoor test facility top view, Figure S3: Monitoring devices in WILD station, Figure S4: Morphology of the nanostructured pseudo-boehmite, Equation (1): equation to calculate the thickness of the pseudo-boehmite as a function of boiling time, Figure S5: FTIR-ATR spectra of bare aluminium alloy, boiled aluminium alloy and SH-1, Figure S6: FTIR-ATR spectra of HP; Figure S7: Images of static contact angles and tilting angles (RA or SA) for SH, HP, SL-1 and SL-2, Table S1: Meteorological and physical data recorded in WILD station during the snowfall events.

Author Contributions: Conceptualisation, M.B.; methodology, M.B. and M.L.; investigation, M.B., G.S.d.M., F.P. and A.C. (Andrea Cammi); resources, M.B. and V.R.; data curation, G.S.d.M., A.C. (Alessandro Casali), F.P. and A.C. (Andrea Cammi), V.R.; writing—original draft preparation, M.B.; writing—review and editing, M.L., G.S.d.M. and A.C. (Alessandro Casali). All authors have read and agreed to the published version of the manuscript.

Funding: This work has been financed by the Research Fund for the Italian Electrical System under the Three-Year Research Plan 2022-2024 (DM MITE n. 337, 15.09.2022), in compliance with the Decree of 16 April 2018.

Institutional Review Board Statement: Not applicable.

Informed Consent Statement: Not applicable.

Data Availability Statement: Not applicable.

Acknowledgments: The authors would like to thank P. Marcacci, C. Chemelli and G. Quinteri for their supporting activity.

Conflicts of Interest: The authors declare no conflict of interest.

References

1. Farzaneh, M. *Atmospheric Icing of Power Networks*; Springer Science & Business Media: Berlin/Heidelberg, Germany, 2008.
2. Fikke, S.M.; Ronsten, G.; Heimo, A.; Kunz, S.; Ostrozlik, M.; Persson, P.; Sabata, J.; Wareing, B.; Wichura, B.; Chum, J.; et al. *COST 727: Atmospheric Icing on Structures: Measurements and Data Collection on Icing: State of the Art*; Meteo Schweiz: Zürich, Switzerland, 2006.
3. Wareing, B.; Nygaard, B. WRF Simulation of Wet Snow and Rime Icing Incidents in the UK. In Proceedings of the 13th International Workshop on Atmospheric Icing of Structures, METEOTEST, Andermatt, Switzerland, 8–11 November 2009.
4. Mc Innes, H.; Haugen, J.E.; Kristjánsson, J.E.; Nygaard, B.E.K.; Rasmussen, R.; Solberg, S.; Blennow, K.; Tveito, O.E. Wind Ice and Snow Load Impacts on Infrastructure and the Natural Environment (WISLINE). In Proceedings of the 19th EGU General Assembly, Vienna, Austria, 23–28 April 2017.
5. Bonanno, R.; Lacavalla, M.; Sperati, S. A New High-Resolution Meteorological Reanalysis Italian Dataset: MERIDA. *Q. J. R. Meteorol. Soc.* **2019**, *145*, 1756–1779. [CrossRef]
6. Farzaneh, M.; Jakl, F. *Coatings for Protecting Overhead Power Network Equipment in Winter Conditions: Working Group B2. 44*; Cigré: Paris, France, 2015.
7. Kreder, M.J.; Alvarenga, J.; Kim, P.; Aizenberg, J. Design of Anti-Icing Surfaces: Smooth, Textured or Slippery? *Nat. Rev. Mater.* **2016**, *1*, 1–15. [CrossRef]

8. Sojoudi, H.; Wang, M.; Boscher, N.D.; McKinley, G.H.; Gleason, K.K. Durable and Scalable Icephobic Surfaces: Similarities and Distinctions from Superhydrophobic Surfaces. *Soft Matter* **2016**, *12*, 1938–1963. [CrossRef]
9. Noormohammed, S.; Sarkar, D.K. Rf-Sputtered Teflon®-Modified Superhydrophobic Nanostructured Titanium Dioxide Coating on Aluminum Alloy for Icephobic Applications. *Coatings* **2021**, *11*, 432. [CrossRef]
10. Wang, N.; Xiong, D.; Lu, Y.; Pan, S.; Wang, K.; Deng, Y.; Shi, Y. Design and Fabrication of the Lyophobic Slippery Surface and Its Application in Anti-Icing. *J. Phys. Chem. C* **2016**, *120*, 11054–11059. [CrossRef]
11. Wang, Z.; Lin, B.; Sheng, S.; Tan, S.; Wang, P.; Tao, Y.; Liu, Z.; He, Z.; Wang, J. Bioinspired Anti-Icing Hydrogel Enabled by Ice-Nucleating Protein. *CCS Chem.* **2022**, *4*, 104–111. [CrossRef]
12. Liu, J.; Zhu, C.; Liu, K.; Jiang, Y.; Song, Y.; Francisco, J.S.; Zeng, X.C.; Wang, J. Distinct Ice Patterns on Solid Surfaces with Various Wettabilities. *Proc. Natl. Acad. Sci. USA* **2017**, *114*, 11285–11290. [CrossRef]
13. Bai, G.; Gao, D.; Liu, Z.; Zhou, X.; Wang, J. Probing the Critical Nucleus Size for Ice Formation with Graphene Oxide Nanosheets. *Nature* **2019**, *576*, 437–441. [CrossRef]
14. Dhyani, A.; Choi, W.; Golovin, K.; Tuteja, A. Surface Design Strategies for Mitigating Ice and Snow Accretion. *Matter* **2022**, *5*, 1423–1454. [CrossRef]
15. *ISO 19403-7:2017*; Paints and Varnishes—Wettability—Part 7: Measurement of the Contact Angle on a Tilt Stage (Roll-off Angle). International Organization for Standardization: Geneva, Switzerland, 2017.
16. Boinovich, L.; Emelyanenko, A.M.; Korolev, V.V.; Pashinin, A.S. Effect of Wettability on Sessile Drop Freezing: When Superhydrophobicity Stimulates an Extreme Freezing Delay. *Langmuir* **2014**, *30*, 1659–1668. [CrossRef]
17. Han Yeong, Y.; Steele, A.; Loth, E.; Bayer, I.; De Combarieu, G.; Lakeman, C. Temperature and Humidity Effects on Superhydrophobicity of Nanocomposite Coatings. *Appl. Phys. Lett.* **2012**, *100*, 053112. [CrossRef]
18. Lacavalla, M.; Marcacci, P.; Chemelli, C.; Balordi, M.; Bonanno, R.; Pirovano, G. Operational Forecast and Research Activities on Wet Snow Accretion in Italy. In Proceedings of the 17th International Workshop on Atmospheric Icing of Structures, Chongqing, China, 25–29 September 2017.
19. Makkonen, L. Models for the Growth of Rime, Glaze, Icicles and Wet Snow on Structures. *Philos. Trans. R. Soc. A* **2000**, *358*, 2913–2939. [CrossRef]
20. Makkonen, L.; Wichura, B. Simulating Wet Snow Loads on Power Line Cables by a Simple Model. *Cold Reg. Sci. Technol.* **2010**, *61*, 73–81. [CrossRef]
21. Sakamoto, Y. Snow Accretion on Overhead Wires. *Philos. Trans. R. Soc. A* **2000**, *358*, 2941–2970. [CrossRef]
22. Bonelli, P.; Lacavalla, M.; Marcacci, P.; Mariani, G.; Stella, G. Wet Snow Hazard for Power Lines: A Forecast and Alert System Applied in Italy. *Nat. Hazards Earth Syst. Sci.* **2011**, *11*, 2419–2431. [CrossRef]
23. Balordi, M.; Cammi, A.; Chemelli, C.; Marcacci, P.; Pirovano, G.; Santucci, G. A Comparison of Anti-Ice and Anti-Snow Coatings Performances: Laboratory and Field Testing. In Proceedings of the International Workshop on Atmospheric Icing of Structures (IWAIS), Reykjavík, Iceland, 23–28 June 2019.
24. Geiculescu, A.C.; Strange, T.F. A Microstructural Investigation of Low-Temperature Crystalline Alumina Films Grown on Aluminum. *Thin Solid Film.* **2003**, *426*, 160–171. [CrossRef]
25. Rider, A.N. The Influence of Porosity and Morphology of Hydrated Oxide Films on Epoxy-Aluminium Bond Durability. *J. Adhes. Sci. Technol.* **2001**, *15*, 395–422. [CrossRef]
26. Motta, A.; Cannelli, O.; Boccia, A.; Zanoni, R.; Raimondo, M.; Caldarelli, A.; Veronesi, F. A Mechanistic Explanation of the Peculiar Amphiphobic Properties of Hybrid Organic–Inorganic Coatings by Combining XPS Characterization and DFT Modeling. *ACS Appl. Mater. Interfaces* **2015**, *7*, 19941–19947. [CrossRef]
27. Balordi, M.; Santucci de Magistris, G.; Chemelli, C. A Novel Simple Anti-Ice Aluminum Coating: Synthesis and In-Lab Comparison with a Superhydrophobic Hierarchical Surface. *Coatings* **2020**, *10*, 111. [CrossRef]
28. Zhong, L.; Chen, X.; Song, H.; Guo, K.; Hu, Z. Highly Flexible Silica Aerogels Derived from Methyltriethoxysilane and Polydimethylsiloxane. *New J. Chem.* **2015**, *39*, 7832–7838. [CrossRef]
29. Vadnere, M.; Amidon, G.; Lindenbaum, S.; Haslam, J.L. Thermodynamic Studies on the Gel-Sol Transition of Some Pluronic Polyols. *Int. J. Pharm.* **1984**, *22*, 207–218. [CrossRef]
30. Chen, D.; Gelenter, M.D.; Hong, M.; Cohen, R.E.; McKinley, G.H. Icephobic Surfaces Induced by Interfacial Nonfrozen Water. *ACS Appl. Mater. Interfaces* **2017**, *9*, 4202–4214. [CrossRef] [PubMed]
31. Ochoa, M.; Durães, L.; Beja, A.M.; Portugal, A. Study of the Suitability of Silica Based Xerogels Synthesized Using Ethyltrimethoxysilane and/or Methyltrimethoxysilane Precursors for Aerospace Applications. *J. Sol-Gel Sci. Technol.* **2012**, *61*, 151–160. [CrossRef]
32. Al-Oweini, R.; El-Rassy, H. Synthesis and Characterization by FTIR Spectroscopy of Silica Aerogels Prepared Using Several Si (OR) 4 and R″ Si (OR′) 3 Precursors. *J. Mol. Struct.* **2009**, *919*, 140–145. [CrossRef]
33. Cassie, A.B.D.; Baxter, S. Wettability of Porous Surfaces. *Trans. Faraday Soc.* **1944**, *40*, 546. [CrossRef]
34. Wenzel, R.N. Resistance of Solid Surfaces to Wetting by Water. *Ind. Eng. Chem.* **1936**, *28*, 988–994. [CrossRef]
35. Niemelä-Anttonen, H.; Koivuluoto, H.; Tuominen, M.; Teisala, H.; Juuti, P.; Haapanen, J.; Harra, J.; Stenroos, C.; Lahti, J.; Kuusipalo, J.; et al. Icephobicity of Slippery Liquid Infused Porous Surfaces under Multiple Freeze–Thaw and Ice Accretion–Detachment Cycles. *Adv. Mater. Interfaces* **2018**, *5*, 1800828. [CrossRef]

36. Karmouch, R.; Ross, G.G. Experimental Study on the Evolution of Contact Angles with Temperature near the Freezing Point. *J. Phys. Chem. C* **2010**, *114*, 4063–4066. [CrossRef]
37. Farhadi, S.; Farzaneh, M.; Kulinich, S.A. Anti-Icing Performance of Superhydrophobic Surfaces. *Appl. Surf. Sci.* **2011**, *257*, 6264–6269. [CrossRef]
38. Heydari, G.; Moghaddam, M.S.; Tuominen, M.; Fielden, M.; Haapanen, J.; Mäkelä, J.M.; Claesson, P.M. Wetting Hysteresis Induced by Temperature Changes: Supercooled Water on Hydrophobic Surfaces. *J. Colloid Interface Sci.* **2016**, *468*, 21–33. [CrossRef]
39. Newby, G.E.; Hamley, I.W.; King, S.M.; Martin, C.M.; Terrill, N.J. Structure, Rheology and Shear Alignment of Pluronic Block Copolymer Mixtures. *J. Colloid Interface Sci.* **2009**, *329*, 54–61. [CrossRef]
40. Susoff, M.; Siegmann, K.; Pfaffenroth, C.; Hirayama, M. Evaluation of Icephobic Coatings—Screening of Different Coatings and Influence of Roughness. *Appl. Surf. Sci.* **2013**, *282*, 870–879. [CrossRef]
41. Wang, Y.; Xue, J.; Wang, Q.; Chen, Q.; Ding, J. Verification of Icephobic/Anti-Icing Properties of a Superhydrophobic Surface. *ACS Appl. Mater. Interfaces* **2013**, *5*, 3370–3381. [CrossRef] [PubMed]
42. Bharathidasan, T.; Kumar, S.V.; Bobji, M.; Chakradhar, R.; Basu, B.J. Effect of Wettability and Surface Roughness on Ice-Adhesion Strength of Hydrophilic, Hydrophobic and Superhydrophobic Surfaces. *Appl. Surf. Sci.* **2014**, *314*, 241–250. [CrossRef]
43. Yang, S.; Xia, Q.; Zhu, L.; Xue, J.; Wang, Q.; Chen, Q. Research on the Icephobic Properties of Fluoropolymer-Based Materials. *Appl. Surf. Sci.* **2011**, *257*, 4956–4962. [CrossRef]
44. Fu, Q.; Wu, X.; Kumar, D.; Ho, J.W.; Kanhere, P.D.; Srikanth, N.; Liu, E.; Wilson, P.; Chen, Z. Development of Sol–Gel Icephobic Coatings: Effect of Surface Roughness and Surface Energy. *ACS Appl. Mater. Interfaces* **2014**, *6*, 20685–20692. [CrossRef]
45. Meuler, A.J.; Smith, J.D.; Varanasi, K.K.; Mabry, J.M.; McKinley, G.H.; Cohen, R.E. Relationships between Water Wettability and Ice Adhesion. *ACS Appl. Mater. Interfaces* **2010**, *2*, 3100–3110. [CrossRef] [PubMed]
46. Jafari, R.; Momen, G.; Eslami, E. Fabrication of Icephobic Aluminium Surfaces by Atmospheric Plasma Jet Polymerisation. *Surf. Eng.* **2019**, *35*, 450–455. [CrossRef]
47. Marcacci, P.; Lacavalla, M.; Pirovano, G. Monitoring, Measurements and Mitigation for Wet Snow Accretion on Overhead Conductors. In Proceedings of the International Workshop on Atmospheric Icing of Structures (IWAIS), Reykjavík, Iceland, 23–28 June 2019.

Disclaimer/Publisher's Note: The statements, opinions and data contained in all publications are solely those of the individual author(s) and contributor(s) and not of MDPI and/or the editor(s). MDPI and/or the editor(s) disclaim responsibility for any injury to people or property resulting from any ideas, methods, instructions or products referred to in the content.